Reducing lock in thermography testing time in photovoltaic cells using thermal transient data

Renan O. Silva[1], Douglas B. Riffel[1]
[1]Federal University of Sergipe (UFS), São Cristóvão (Brazil)

Abstract

Lock-in Thermography is a technique used in non-destructive testing to characterize defects in various materials, including electronic components and photovoltaic cells. In this type of thermography, tests are performed using a periodic signal that heats the photovoltaic cells for a long period of time, since the analysis is performed when the material reaches a steady state temperature. This work proposes a method to reduce test time, based on adjusting a curve with the thermal transient data of temperature generated during heating to estimate the thermal information of the material in steady state. Thus, after data processing, it is possible to obtain images that represent the internal behavior of the material similar to those obtained using the classical method. To compare these images, a similarity index is used, quantitatively measuring how close the image generated is to the image obtained in steady state. The use of the proposed method allowed obtaining images that represent the characteristics of the cells studied, as well as obtained in steady state, reducing the test time by approximately 80%.

Keywords: Lock-in thermography, thermal transient, fast Fourier transform, structural similarity index measure

1. Introduction

Given the projected growth of the renewable energy market for the coming years, in addition to installations that have been operating for some time, the continuous development of technologies is necessary, among other reasons, to ensure the proper functioning of photovoltaic installations. In this sense, techniques to monitor and identify failures in solar panels before installation or during periodic inspections allow the systems to operate with a significant reduction in performance losses (Kingma et al., 2021).

There are several non-destructive techniques for monitoring photovoltaic systems and identifying faults, the main ones being the electrical method of measuring the I-V characteristic curve of modules and imaging methods such as infrared thermography and electroluminescence (Mellit et al, 2018). These techniques allow for the identification of faults caused during cell or module production, transportation and installation, such as cracks, hot spots, shunts, potential-induced degradation (PID), among others. However, the use of characteristic curve does not allow defects identified by I-V data to indicate the exact location in the cell, explaining the origin of the problem (Guo and Cai, 2021). This is possible with imaging methods, with infrared thermography being a well-established method in this regard (Breitenstein and Langenkamp, 2010; Asadpour et al., 2020).

Among the types of thermography most commonly used to characterize defects in photovoltaic cells, Lock-in Thermography is a technique in which the sample is periodically heated through electrical excitation with a modulated signal and its temperature variation on the surface is evaluated through signal processing techniques such as the Fast Fourier Transform (FFT) (Breitenstein and Langenkamp, 2010).

However, as a disadvantage, Lock-in thermography requires several cycles to reach the permanent heating regime in order to obtain adequate results, since this technique needs to be evaluated in this regime (Breitenstein and Langenkamp, 2010). This means that tests using this technique take long periods of time, depending on the material under study, becoming a factor that greatly interferes in the characterization of photovoltaic cells and modules.

10.18086/swc.2025.03.64 Available at http://proceedings.ises.org

One solution suggested in some studies to reduce this test time would be to analyze the transient heating regime to obtain representative images of the material under study (Chatterjee and Tuli, 2012; Luo et al., 2023; Matarrese et al., 2023). Thermal data is modeled using a mathematical function to represent the material's heating curve, using a polynomial to model the transient component and a sinusoidal waveform for the steady state. This model can be used to preprocess the data, removing the portion of the signal influenced by the transient, leaving only the oscillatory component (Stoynova and Bonev, 2018), or to generate amplitude and phase images by applying data post-processing techniques (FFT, 4P, SR, among others) from the curve fitted to the experimentally obtained data (Chatterjee and Tuli, 2012; Luo et al., 2023; Matarrese et al., 2023).

This work proposes a method to reduce the time of the lock-in thermography test without reducing the ability to detect defects in photovoltaic cells. The aim is to synthesize images through a shorter test, that is, using data from the transient regime, in the expectation of obtaining representative images of the internal functioning of the cell, using values extrapolated from an adjusted model.

2. Materials and Methods

2.1. Experimental Setup

The experimental setup of lock-in thermography listed in Vieira et al. (2023) was used as a basis in this work. This setup presents a function generator (model Keysight 33250) that generates sinusoidal waves to power the cell and make it heat up, according to the current signal inserted into its terminals and in a reverse way as it functions in solar panels. This signal needs to be amplified with a power amplifier circuit to power the solar cell because of the limitation of the function generator, given the current required to heat the cell adequately. The cell under study is inside a darkroom, to minimize interference from electromagnetic radiation. The whole setup is presented in Fig. 1.

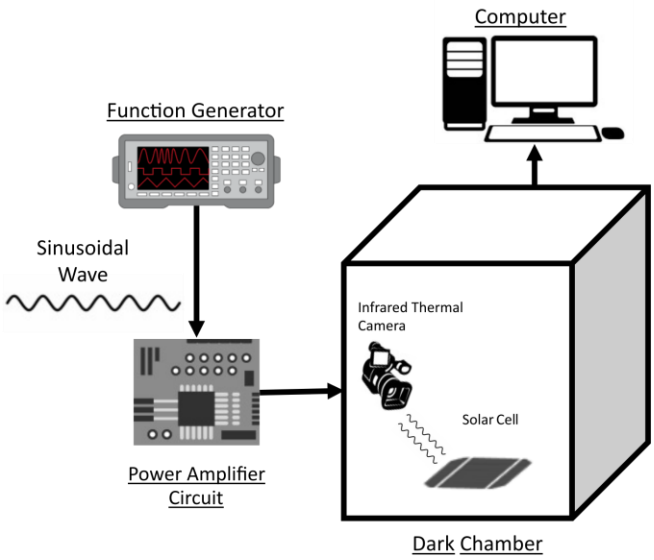

Figure 1: Setup used in this work for the tests on the solar cells.

Also, the same type of photovoltaic cells (SunPower™ C60 monocrystalline with 3.4 Wp and dimensions of 12.5 × 12.5 cm², short circuit current, I_{CC}, of 6.27A and an open circuit voltage, V_{AC}, of 0.68V) under different conditions (one healthy and two with distinct defects) were used (figure 2, a-c). To determine the condition of the cells, electroluminescence tests were performed to assess whether they were healthy or not and to identify the locations of the defects (Fig. 2, d-f).

In the defective cell (cell nº 2) shown in Figure 2b the defects were created manually by pressing and twisting the cell. This procedure created a diagonal crack, almost causing the cell to fold, along with others minor fractures. The electroluminescence test (Fig. 2e) revealed that most of the cell area was inactive (dark areas), with only two regions operating as expected. In the last cell (cell nº 3), defects appeared after the soldering process of the terminals in the cell, creating a vertical line pattern in the middle and some minor cracks on the sides, as observed in the electroluminescence image (Fig.2c).

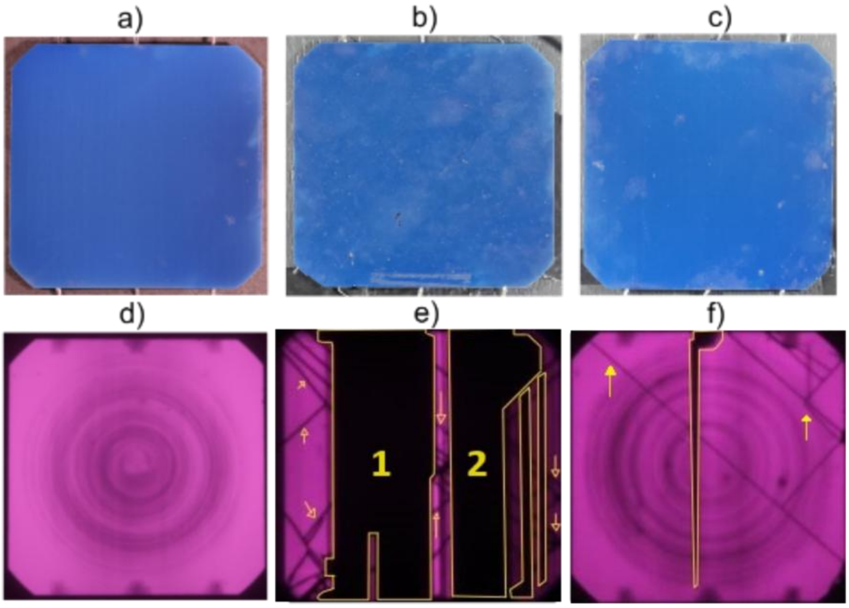

Figure 2: Solar cells used in this work and their respective images of electroluminescent tests. a) is the healthy cell, b) and c) are the defectives, with the defects highlighted.

The tests were performed by exciting the cell with a sinusoidal signal for an interval of 55 minutes, ensuring that the cell's permanent heating regime was reached. It was used three different signal frequencies (11, 50 and 100 mHz), performing five tests for each cell (total of 45 tests). The tests were recorded using an IR camera (FLIR T420), with the emissivity factor of 0.74, and the FLIR Atlas SDK, using the USB interface and MATLAB software to store the temperature data in radiometric videos. The computer used in the tests has a Intel Xeon E3-1240 v3 @ 3.40GHz processor, 32 GB RAM memory, Windows 10 operational system and MATLAB®, version R2018b.

2.2. Data processing and procedure to obtain and analyse amplitude and phase images

Using radiometric videos obtained from the tests, temperature data can be processed to generate images that indicate the presence or absence of defects. Following the traditional process, data from the permanent regime (the moments closest to the end of the video) are used for the evaluation. However, in this work, the video was divided into several parts, each lasting a period of the excitation frequency, to assess the possibility of using a video from a shorter test to obtain defect information, as in the standard procedure.

For the procedure used in this work, the first step defined was to divide the video into parts, each of them with the same duration as the period of the excitation wave used in the test. These parts are then processed to provide temperature data for the cell region in the video, segmenting this area of interest. The FFT is applied to the temperature data obtained in the last step to generate amplitude and phase images, which are used to verify the presence of defects in the cell for all parts obtained for each test realized. The images obtained have dimensions of 200x200 pixels, with the cell centered and had their minimum and maximum values adjusted to improve contrast and, consequently, visualization.

2.3. A robust procedure to obtain images from a reduced-size video

In order to identify defects while reducing the test time, the proposed method uses the data from the first ten minutes of the tests, without waiting for the cell to reach a stable thermal regime. The tests were recorded up to 55 minutes in accordance with the standard procedure, but just to obtain reference images for comparation with those obtained using the proposed method. Part of these shorter temperature data are adjusted to a curve using an equation (eq. 1) on the MATLAB® fit function.

$$\mathrm{T(t)} = T_0 + \Delta\mathrm{T}\left(1 - e^{-\frac{t}{\tau}}\right) + \mathrm{A}\sin(2\pi f_L t + \varphi) \qquad \text{(eq. 1)}$$

where T_0 is the initial temperature of a pixel, ΔT is the variation in thermal amplitude, τ is the time constant, f_L is the lock-in frequency and φ is the phase shift for the excitation signal.

Once the coefficients of the curve adjusted to the data have been obtained, they are used to estimate the temperature values in each pixel in a period of time in which the cell would be in a stable regime, creating a temperature matrix similar to that obtained after extracting the data from the thermographic video. With this matrix in hand, it is possible to proceed and apply the processing techniques to obtain the synthesized amplitude and phase images, which are compared with the image obtained in standard procedure (result of subsection 2.2) as the reference image using an image quality index (structural similarity index measure - SSIM).

A robust method to ensure the synthesis of images that represent the situation of the cell under study is proposed. A diagram representing the steps of the process is shown in Fig. 3. The test video is divided into intervals, based on the period of the excitation signal of the thermographic test. Each interval has a temperature matrix and a mask, which indicates the area of interest. Images are obtained for each interval using the FFT. Then, each image of a type (amplitude or phase) is used as a reference and compared with all others of the same type to verify their similarity. In this way, it is possible to create a matrix with the values of these indexes and verify the average similarity of each image to the others. The highest averages are chosen, based on the number of periods to obtain approximately five minutes of video (3 periods for 11 mHz, 15 for 50 mHz and 30 for 100 mHz) and then the temperature matrices of the chosen periods are concatenated in increasing order of their appearance in the video, to create an improved signal without periods in which the obtained images were dissimilar. A curve is adjusted based on the signal obtained in this previous step and a temperature matrix is created estimating the data in the steady state (55 minutes of the test) using the coefficients of the adjusted curve. The amplitude and phase images are synthesized by applying the FFT to the temperature matrix from the adjusted curve.

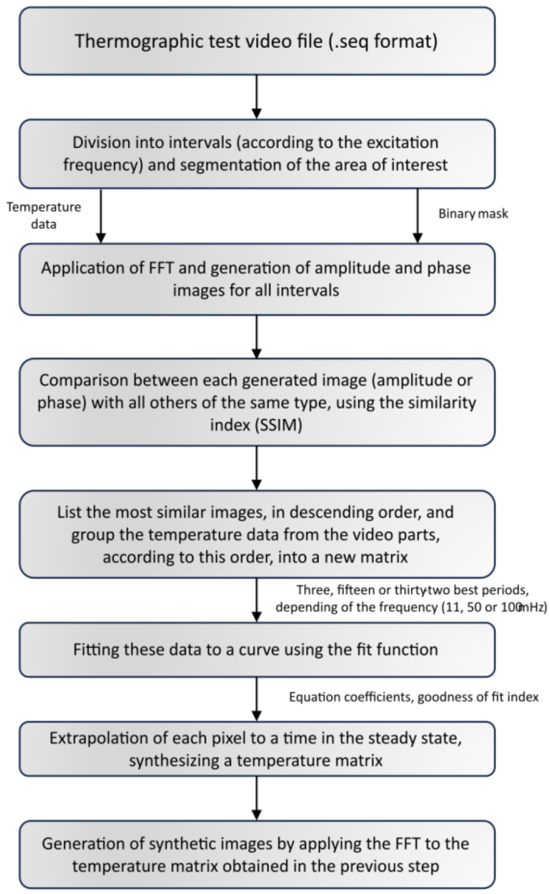

Figure 3: Flowchart showing the steps of the robust method for synthesizing amplitude and phase images from modulated active thermography tests.

3. Results and Discussion

3.1. Comparison between synthesized images and those obtained experimentally

Using the data from the 45 videos of the experiments (for each of the 05 tests made for the each of the 03 cells and 03 frequencies), images were obtained to characterize the behavior of the cells and the developed method was applied to the data and the results were analyzed. This subsection will present the results for the images obtained in the standard procedure, using data from permanent regime, and for the synthesized, making a comparison between them.

By applying data processing and using FFT in the thermographic tests, images representing the internal behavior of the tested cells were obtained. Fig. 4 shows images resulting from this procedure for some of the tests performed, where red areas indicate heating of the cell while blue show cooler areas. It can be seen that the cell considered healthy has a circular pattern of thermal distribution (in the case of the amplitude image, Figure 4a) as well as of phase distribution between adjacent points of the image (in the case of the phase images, Fig. 4d).

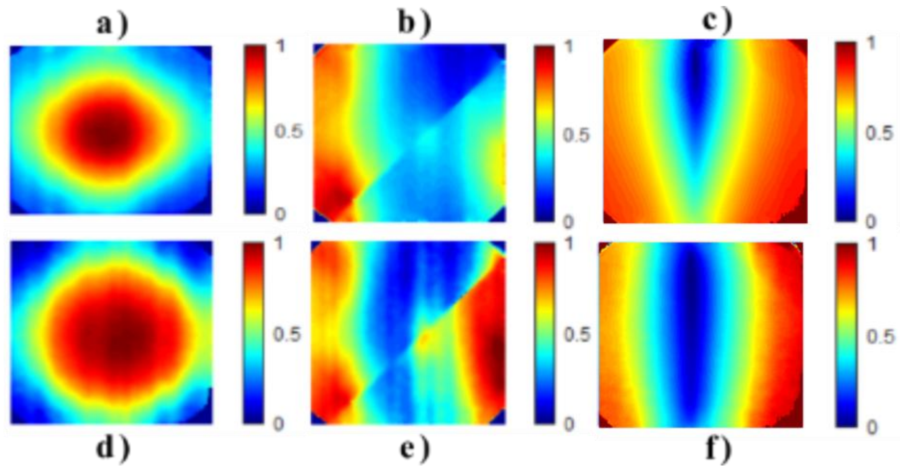

Fig. 4: Amplitude (a to c) and phase (d to f) images of the cells indicating their internal behavior. Images a) and d) were obtained from the healthy cell (nº1), b) and e) from the defective cell (nº2) and c) and f) from the defective cell (nº3).

For defective cells, the pattern of the images obtained is different, highlighting the regions where there is inactivity in the cell (blue areas in Fig. 4), mainly for the phase images, as reported in Vieira et al. (2023). This information can be visualized by comparing it with the regions in the electroluminescence images where no light emission occurs (areas in black, in Fig. 2, d-f), indicating the defective area. It can be seen that for the cell nº2 (Fig. 4b and 4e) only the side areas of the images show some heating, corresponding to the result of the electroluminescence test, For the cell nº3, the amplitude and phase images (Fig. 4c and 4f) shows heating around the vertical defect in the central area, making a change in the expected shape as in a healthy cell.

Using the image synthesis procedure defined in the methodology, the images were successfully synthesized, representing the internal behavior of the cells from which the synthesis data were used. Fig. 5 shows some examples of the amplitude (Fig. 5g, 5i and 5k) and phase (Fig. 5h, 5j and 5l) images obtained using this procedure.

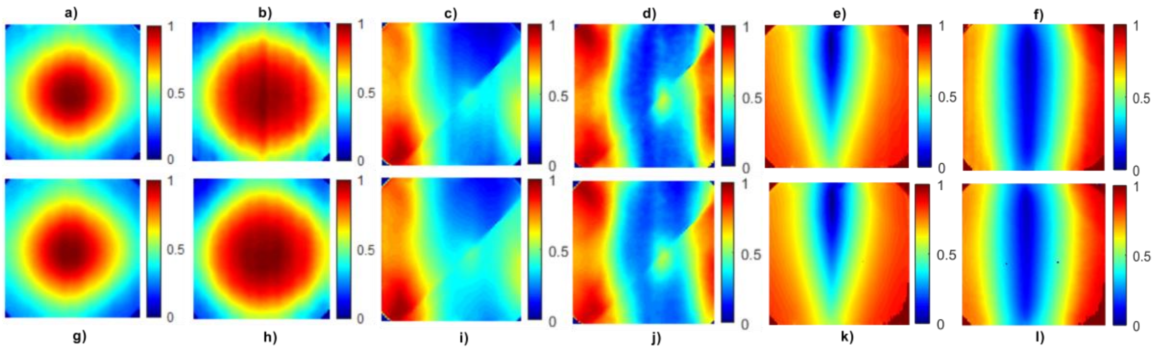

Fig. 5: Images of the cells indicating their internal behavior. Images a), b), g) and h) were obtained from the healthy cell (nº1); c), d), i) and j) from the defective cell (nº2) and e), f), k) and l) from the defective cell (nº3).

Comparing the images, it was qualitatively verified that the synthesized images obtained closely resemble the reference images, obtained experimentally with the data from the steady state of the tests. An example is shown in Fig. 5, with b), d) and f) were the phase images of the cells obtained with the standard procedure and h), j) and l) the synthesized ones. By comparing both images, it is possible to characterize the cells internal behavior, showing a small variation in the size of the areas. Another finding is that in the synthesized ones the image appears to be less noisy. This is due to the data smoothing performed in the curve fitting stage.

To obtained values that demonstrate its quality of the synthesis, the coefficient of determination R^2 and the mean squared error were used, obtained for each pixel of the image and then an overall average, in the fitting procedure applied to the data. The values found are summarized in Table 1. The R^2 coefficients, obtained for the tests performed on the healthy cell, are greater than 0.9 (varies between 0 and 1) for the frequencies used (11, 50, and 100 mHz). The mean squared error varied between 0.09°C and 0.16°C. These values demonstrate that it was possible to achieve a good fit of the model, with a high R^2 coefficient combined with a low squared error, since the temperature variation in the tests has values greater than 1.5°C (an error of approximately 10% in the worst case). For the defective cells, the fit coefficient values were lower than for the healthy cell, except at the 11 mHz frequency of the cell nº3. Combined with a slightly larger mean squared error, this demonstrates some difficulty in fitting compared with the healthy cell. Despite the lower values of the fitting coefficients, most of the images obtained represented the existing defects.

Table 1: Mean quality index of the synthesized images for the tests realized with the three cells.

Cell	Frequency of the tests		
	11 mHz	50 mHz	100 mHz
Cell 01 - Healthy	R^2 - 0,9060	R^2 - 0,9309	R^2 - 0,9487
	RMS – 0,0907º	RMS – 0,1608º	RMS – 0,1261º
Cell 02 - Defective	R^2 - 0,8286	R^2 - 0,7491	R^2 - 0,8019
	RMS – 0,1180º	RMS – 0,1394º	RMS – 0,1931º
Cell 03 - Defective	R^2 - 0, 9414	R^2 - 0, 8482	R^2 - 0, 9035
	RMS – 0, 1607º	RMS – 0, 2662º	RMS – 0, 1531º

In general, the indices obtained were very similar, especially for the amplitude images, with a greater variation as the frequency increases. In Table 2, It is possible to see that in Cell 01 - Health, the mean SSIM is between 0.9696 (100 mHz) and 0.9896 (11 mHz); in Cell 02 - Defective, between 0,8910 (100 mHz) and 0,9735 (11 mHz) and in Cell 03 – Defective, between 0.8126 (100 mHz) and 0.9949 (11 mHz).

Table 2: Mean similarity index of the synthesized images for the tests realized with the three cells, with and without the proposed method.

Cell	Mean similarity index (SSIM) of the tests per frequency						
	Type of image	11 mHz		50 mHz		100 mHz	
		Standard Synthesis	Proposed Method	Standard Synthesis	Proposed Method	Standard Synthesis	Proposed Method
Cell 01 - Healthy	Amplitude	0,9896	0,9898	0,9934	0,9948	0,9696	0,9737
	Phase	0,9423	0,9604	0,9256	0,9739	0,9132	0,9309
Cell 02 - Defective	Amplitude	0,9735	0,9948	0,9843	0,9628	0,8910	0,8774
	Phase	0,9292	0,9739	0,9058	0,9669	0,8173	0,8397
Cell 03 - Defective	Amplitude	0,9949	0,9737	0,9563	0,9831	0,8126	0,9323
	Phase	0,9681	0,9309	0,9374	0,9215	0,6743	0,8820

However, in the phase images of the defective cells, at frequencies of 50 and 100 mHz, some problems were found in the adjustment, especially for cell 03 (mean SSIM of 0.6785), generating images that did not characterize the defect correctly (Fig. 6b). Analyzing the problem and performing some tests, it was possible to notice that depending on the data used in the adjustment (whether they were closer to the beginning or end of the transient), the synthesized image improved the index and presented the expected behavior or, at least, closer to the reference (as seen in the Fig. 6c). Thus, the choice of data was necessary to generate more robust results for the solution.

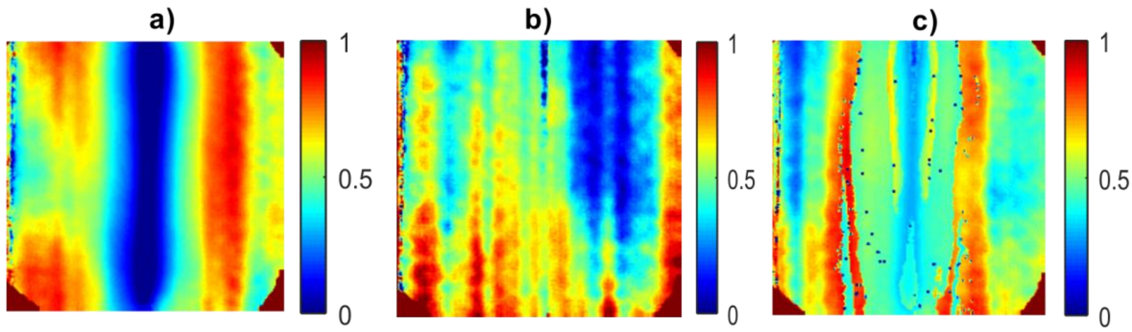

Fig. 6: Comparation of phase images of the cell n°3. a) Image obtained with the steady-state data (100 mHz). b) Synthesized with transient data (without choosing the best data). c) Synthesized with the robust method.

3.2. Results of the robust method for Lock-in thermography image synthesis

Using data from previously performed tests and applying the proposed method to obtain amplitude and phase images in reduced-time tests, it was possible to get images that were closer to the reference in most of the tests. In Fig. 6c, it is possible to see that the defect region appears in the image, unlike the image generated without the method. It presents a meaningful result, although it's not very close to what was expected. In Fig. 7c, it is possible to see that the regions are closer to the reference image than for the synthesis without using the method (Fig. 7b).

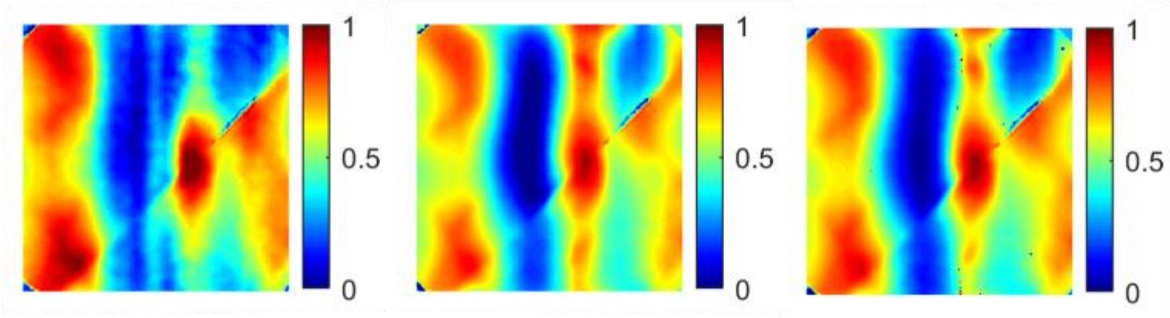

Fig. 7: Phase images of the cell nº2 indicating the defective area in blue. a) Image obtained with the steady-state data (100 mHz). b) Synthesized with transient data (without choosing the best data). c) Synthesized with the robust method.

In Table 2, for cell 01, it was possible to verify that the images for all frequencies obtained a similarity index above 0.91, indicating images very similar to the reference in the steady state. Also, thirteen synthesized images of eighteen with this method had better results (72.22%) than for the synthesis without using the method. In cells 02 and 03, the use of the method generated images that represented the defects, correcting the problem found in the common synthesis. In some cases, such as the one marked in green in the table, the indices obtained were much higher, especially for the phase images, where the mean index got 14,73% and 30,8% improved, respectively. And, looking for each test done, 80% of the phase images in cell 2 and 60% in cell 3 improved. This behavior is also due to the choice of the most similar periods when adjusting the model, since, probably in these tests, the first periods did not have good similarity with the reference image, and with the possibility of choosing the best ones from the entire transient, it was possible to eliminate them when selecting the data for adjustment.

4. Conclusion

This work investigated a way to reduce the time of lock-in thermography tests applied to photovoltaic cells, using information obtained during the thermal transient of heating. The adjustment of the transient data to obtain the models was successful in synthesizing both amplitude and phase images.

In the qualitative analyses, the images obtained presented more homogeneous regions than those obtained in the experiments, with a great reduction of noise in the image, as seen in other studies (Chatterjee and Tuli, 2012; Luo et al., 2023; Matarrese et al., 2023). In quantitative terms, averaging the indices of the comparison between these images and the steady state images obtained experimentally, it is noted that those based on curve adjustment not only manage to identify the defects but also have a similarity index close to the reference, proving to be a reliable way of characterize the defects. Furthermore, it reduces the test time, as it only uses a maximum of 12 minutes, as opposed to the 55 minutes that is generally used (a 78.2% reduction in time).

Using the robust method on the same data used previously allowed us to observe that, in most cases, choosing the periods by comparing the similarity of the images between themselves allowed for the generation of images that were closer to the steady state images than without the use of the method. Furthermore, its use made it possible to generate images that represent the defects in the cell in cases where this was not possible, excluding or reducing the influence of the noisy thermal information from these tests.

5. Acknowledgments

The authors gratefully acknowledge the financial support provided by FAPITEC (Foundation for the Support of Research and Technological Innovation of the State of Sergipe).

6. References

Asadpour, R.; Sulas-Kern, D. B.; Johnston, S.; Meydbray, J. and Alam, M. A., 2020. Dark Lock-in Thermography Identifies Solder Bond Failure as the Root Cause of Series Resistance Increase in Fielded Solar Modules. IEEE Journal of Photovoltaics, vol. 10, no. 5, pp. 1409-1416.

Breitenstein, W. W. O.; Langenkamp, M., 2010. Lock-in Thermography: Basics and Use for Evaluating

Electronic Devices and Materials. 2nd. ed. [S.l.]: Springer Berlin, Heidelberg. ISBN 978-3-642-02416-0, 978-3-642-02417-7.

Chatterjee, K.; Tuli, S., 2012. Image enhancement in transient lock-in thermography through time series reconstruction and spatial slope correction. IEEE Transactions on Instrumentation and Measurement, v. 61, n. 4, p. 1079–1089.

Guo, X.; Cai, J., 2021. Optical stepped thermography of defects in photovoltaic panels. IEEE Sensors Journal, v. 21, n. 1, p. 490–497.

Kingma, A.; Naziris, F.; Bakker, K.; Mack, K.; Huhn, V. and Theelen, M., 2021. Study of the physical and chemical origin of features observed in luminescence and thermography images of cu(in,ga)se2. Solar Energy Materials and Solar Cells, v. 230, p. 111145. ISSN 0927-0248.

Luo, Z.-T.; Shen, P.; Ren, Y.; Wu, Y-S.; Luo, H.; Zheng, K. and Zhang, H., 2023. Nondestructive inspection of subsurface defects in metals by transient lock-in thermography. In: IEEE. 2023 IEEE Far East NDT New Technology & Application Forum (FENDT). [S.l.]. p. 66–70.

Matarrese, T.; Palumbo, D.; Galietti, U., 2023. Comparison in the transient regime of four lock-in thermography algorithms by means of synthetic and experimental data on CFRP. NDT & E International, v. 139, p. 102925.

Mellit, A.; Tina, G.; Kalogirou, S., 2018. Fault detection and diagnosis methods for photovoltaic systems: A review. Renewable and Sustainable Energy Reviews, v. 91, p. 1–17. ISSN 1364-0321.

Stoynova, A. V.; Bonev, B. B, 2018. Improvement the post-processing quality in lock-in thermography. In: International Journal of Circuits, Systems and Signal Processing.

Vieira, T. M.; Santana, E. C.; Souza, L. F. S.; Silva, R. O.; Ferreira, T. V. and Riffel, D. B., 2023. A novel experimental procedure for lock-in thermography on solar cells. AIMS Energy, v. 11, n. 3, p. 503–521. ISSN 2333-8334.